

A cyclic time-dependent Markov process to model daily patterns in wind turbine power production

Teresa Scholz^a, Vitor V. Lopes^{a,*}, Ana Estanqueiro^a

^a*LNEG, National Laboratory for Energy and Geology, Estrada do Paço do Lumiar, 22, 1649-038, Lisboa, Portugal*

Abstract

Wind energy is becoming a top contributor to the renewable energy mix, which raises potential reliability issues for the grid due to the fluctuating nature of its source. To achieve adequate reserve commitment and to promote market participation, it is necessary to provide models that can capture daily patterns in wind power production. This paper presents a cyclic inhomogeneous Markov process, which is based on a three-dimensional state-space (wind power, speed and direction). Each time-dependent transition probability is expressed as a Bernstein polynomial. The model parameters are estimated by solving a constrained optimization problem: The objective function combines two maximum likelihood estimators, one to ensure that the Markov process long-term behavior reproduces the data accurately and another to capture daily fluctuations. A convex formulation for the overall optimization problem is presented and its applicability demonstrated through the analysis of a case-study. The proposed model is capable of reproducing the diurnal patterns of a three-year dataset collected from a wind turbine located in a mountainous region in Portugal. In addition, it is shown how to compute persistence statistics directly from the Markov process transition matrices. Based on the case-study, the power production persistence through the daily cycle is analysed and discussed.

Keywords:

Cyclic Markov process, wind power, persistence, diurnal pattern

*Corresponding author

Email addresses: `teresa.scholz@lneg.pt` (Teresa Scholz), `vitor.lopes@lneg.pt` (Vitor V. Lopes), `ana.estanqueiro@lneg.pt` (Ana Estanqueiro)

1. Introduction

The EC European Parliament objective to achieve 20% of the consumed energy from the renewable energy sector by 2020 introduced a serious challenge to the planning and operating of power systems. Wind energy is becoming a top contributor to the renewable energy mix due to rather high capacities and generation costs that are becoming competitive with conventional energy sources [28]. However, wind energy systems suffer from a major drawback, the fluctuating nature of their source, which affects the grid security, the power system operation and market economics. There are several tools to deal with these issues, such as the knowledge of wind power persistence and wind speed or power simulation. Persistence is related to stability properties and can provide useful information for bidding on the electricity market or to maintain reliability, e.g. by setting reserve capacity.

Wind power or speed simulation can be used to study the impact of wind generation on the power system. For this task, a sufficiently long time series of the power output from the wind plants should be used. However, real data records are commonly of short length and thus synthetic time series are generated by stochastic simulation techniques to model wind activity [16]. Shamshad et al. [23] used first and second-order Markov chain models for the generation of hourly wind speed time series. They found that a model with 12 wind speed states (1 m/s size) can capture the shape of the probability density function and preserve the properties of the observed time series. Additionally, they concluded that a second-order Markov chain produces better results. Nfaoui et al. [15] compared the limiting behavior of their Markov chain model with the data histograms gotten from hourly averaged wind speed and showed that the statistical characteristics were faithfully reproduced. Sahin and Sen [22] reported the use of a first-order Markov chain approach to simulate the wind speed, where: a) both transitions between consecutive times and within state wind speeds are sampled using a uniform distribution; and, b) extreme states are sampled with an exponential distribution. They showed that statistical parameters were preserved to a significant extent; however, second-order Markov chain models could yield improved results.

Although wind power can be computed from synthetic wind speed time series, Papaefthymiou and Klöckl [16] show that a stochastic model using wind power leads to a reduced number of states and a lower Markov chain model order. They compared a Markov chain based method for the direct

38 generation of wind power time series with the transformed generated wind
39 speed. Both the autocorrelation and the probability density function of the
40 simulated data showed a good fit. Thus, they concluded that it is better to
41 generate wind power time series. Chen et al. [7] also modeled wind power by
42 using different discrete Markov chain models: the basic Markov model; the
43 Bayesian Markov model, which considers the transition matrix uncertainty;
44 and, the birth-and-death Markov model, which only allows state transitions
45 between immediately adjacent states. After comparing the wind power au-
46 tocorrelation function, the authors find the Bayesian Markov model best.
47 Lopes et al. [13] proposed a Markov chain model using states that combine
48 information about wind speed, direction and power. From the transition
49 matrix, they compute statistics, such as the stationary power distribution
50 and persistence of power production, which show a close agreement with
51 their empirical analogues. The model was then used for the two-dimensional
52 stochastic modeling of wind dynamics by Raischel et al. [21]. They aim at
53 studying the interactions between wind velocity, turbine aerodynamics and
54 controller action using a system of coupled stochastic equations describing
55 the co-evolution of wind power and speed. They showed that both the de-
56 terministic and stochastic terms of the equations can be extracted directly
57 from the Markov chain model.

58 The knowledge of wind power production persistence provides useful in-
59 formation to run a wind park and to bid on the electricity market, since it
60 provides information about the expected power steadiness. It can be seen
61 as the average time that a system remains in a given state or a subset of
62 states. Existent literature focuses mainly on wind speed persistence, which
63 is used for assessing the wind power potential of a region. Persistence can be
64 determined directly from the data [20, 19]; however, the presence of missing
65 data leads to an underestimate of actual persistence. Alternative methods
66 are based on wind speed duration curves [14, 10], the autocorrelation func-
67 tion or conditional probabilities. Koçak [11] and Cancino-Solórzano et al. [5]
68 compare these techniques, and both conclude that wind speed duration curve
69 yields the best results, i.e. results that follow the geographical and climatic
70 conditions of the analyzed sites. Moreover, Cancino-Solórzano et al. [5] an-
71 alyze the concept of “useful persistence”, which is the time schedule series
72 where the wind speed is between the turbine cut-in and cut-out speed. The
73 results gotten from this analysis coincide with the persistence classification
74 obtained using the speed duration curves. In addition, Koçak [12] suggests a
75 detrended fluctuation analysis to detect long-term correlations and analyze

76 the persistence properties of wind speed records. Sigl et al. [24], Corotis et al.
77 [8] and Poje [19] proposed an approach based on the use of a power law or
78 exponential probability distributions for the persistence of wind speed above
79 and below a reference value. A Markov chain based method to derive the
80 distribution of persistence is introduced by Anastasiou and Tsekos [1], who
81 show its capability on wind speed data.

82 Most methods in literature of wind speed and power synthesis fail to rep-
83 resent diurnal patterns in the artificial data. However, these are relevant for
84 energy system modeling and design, since their knowledge allows to plan and
85 schedule better. For instance, a power production behavior that best matches
86 demand needs smaller reserve capacity. Recently, Suomalainen et al. [26, 25]
87 introduced a method for synthetic generation of wind speed scenarios that
88 include daily wind patterns by sampling a probability distribution matrix
89 based on five selected daily patterns and the mean speed of each day. Cara-
90 pellucci and Giordano [6] adopt a physical-statistical approach to synthesize
91 wind speed data and evaluate the influence of the diurnal wind speed profile
92 on the cross-correlation between produced energy and electrical loads. The
93 parameters of their model, such as diurnal pattern strength or peak hour of
94 wind speed are determined through a multi-objective optimization, carried
95 out using a genetic algorithm.

96 This paper introduces a cyclic time-variant Markov model of wind power,
97 speed and direction designed to consider the daily patterns observed in the
98 data. The model can be used to synthesize data for the three variables
99 and is capable of reproducing the daily patterns. Moreover, it allows to
100 compute persistence statistics depending on the time of the day. The paper is
101 organized as follows: Section 2 introduces the proposed model as an extension
102 of the “regular” Markov chain model, which is then used for comparison.
103 Furthermore it is shown, how to compute the time-of-the-day dependent
104 persistence statistics directly from the Markov model transition matrices.
105 In section 3 the constrained convex optimization problem to get the model
106 parameters is introduced and explained. It is applied to the analysis of a
107 case-study based on real dataset, section 4. Since the model describes the
108 joint statistics for wind power, speed and direction, Section 5 explains how
109 to create synthetic time-series for these variables. Section 6 compares the
110 synthesized data of both the time-variant and the time-invariant versions of
111 the model. Moreover, it is shown how the persistence of power production
112 varies through the daily cycle.

113

114 **Nomenclature**

115 α_0 Initial state distribution at time step $t = 0$

116 $\beta_{\mu}^{i,j}$ Coefficients of the Bernstein polynomial modeling the transition proba-
117 bility $p_{i,j}(t)$

118 $\mathbf{1}_{\mathcal{A}}$ unit column vector of the same size as subset \mathcal{A}

119 \mathbf{P} $P_0 \cdot \dots \cdot P_{T-1}$

120 \mathcal{A} Subset of the state space, containing the states of interest for persistence

121 \mathcal{S} Set of observed state transitions

122 \mathcal{S}_z Set of transitions observed in the data together with the scaled time of
123 the day z at which they are observed

124 ω Weight of the extra transitions added to the objective function

125 π Stationary distribution of a time-invariant Markov chain

126 $\pi^* \lim_{t \rightarrow \infty} \mathbf{P}^t$

127 π_r Stationary distribution at time r of a time-variant cyclic Markov process

128 $\pi_r(j)$ Stationary probability, of state j at time of the day r

129 $\pi_r(\mathcal{A})$ Vector whose elements are the stationary probabilities of the states in
130 the set \mathcal{A} at time of the day r

131 τ Persistence

132 τ_r Time-dependent persistence in a cyclic Markov process

133 $b_{\mu,k}(z)$ μ -th Bernstein basis polynomial of order k

134 $E[\]$ Expected value operator

135 P_t t -th step transition matrix of a Markov process

136 $p_{i,j}(t)$ t -th step transition probability of a Markov process

- 137 $p_{i,j}^{avg}$ Daily average probability of transition from state s_i to s_j
- 138 r_t Remainder of time step t modulo T
- 139 S Markov process state space
- 140 s_i i -th state of a Markov process
- 141 T Period of a cyclic Markov process
- 142 t Time step of a Markov process
- 143 X_t Markov process
- 144 z Scaled time of the day
- 145 $\pi_{\mathcal{A}}$ Stationary probability distribution of the states in subset \mathcal{A}
- 146 r time of the day

147 **2. Time-inhomogeneous Markov model**

148 *2.1. Definition*

149 A discrete finite Markov process $\{X_t \in S, t \geq 0\}$ is a stochastic process
 150 on a discrete finite state space $S = \{s_0, s_1, \dots, s_n\}$, $n \in \mathbb{N}$, whose future
 151 evolution depends only on its current state [9]. This Markov property is
 152 expressed mathematically by

$$Pr\{X_{t+1} = s_j \mid X_t = s_i \wedge X_l \in S \quad \forall l = 0, \dots, t-1\} = Pr\{X_{t+1} = s_j \mid X_t = s_i\}.$$

153

154 $Pr\{X_{t+1} = s_j \mid X_t = s_i\}$ describes the probability of the Markov process
 155 moving to state s_j at time step $t+1$ given that it is in state s_i and is called
 156 the t -th step transition probability, denoted as $p_{i,j}(t)$. Thus, for each time
 157 step t the Markov process has an associated transition probability matrix
 158 P_t , a n by n matrix with entries $[P_t]_{i,j} = p_{i,j}(t)$ for all $i, j \in \{0, \dots, n\}$.
 159 Each P_t satisfies the following properties: $p_{i,j}(t) \geq 0$ and $\sum_j p_{i,j}(t) = 1$
 160 $\forall i, j \in \{0, \dots, n\}$, $\forall t$. A Markov process is called cyclic with period $T \in \mathbb{N}$,
 161 if T is the smallest number, such that $p_{i,j}(mT+r) = p_{i,j}(r)$ for all m in
 162 \mathbb{N} , $0 \leq r < T$ [18]. Thus, a cyclic Markov process is described by T transi-
 163 tion matrices P_r , $r = 0, \dots, T-1$. The remainder of time step t modulo T
 164 will be denoted as r_t and thus $r_t = r_{t+mT} \forall t, m \in \mathbb{N}$.

165 If the transition probabilities are time-independent, i.e. $p_{i,j}(t) = p_{i,j}$, the
 166 process is called a (time-homogeneous) Markov chain and its probability ma-
 167 trix $P \in \mathbb{R}^{n+1 \times n+1}$ is given by $[P]_{i,j} = p_{i,j}$. By analogy to the time-dependent
 168 case it holds that $p_{i,j} \geq 0$ and $\sum_j p_{i,j} = 1 \forall i, j \in \{0, \dots, n\}$.

169

170 *2.2. Communication classes and irreducibility*

171 *2.2.1. Time-invariant Markov chain*

172 The probability of reaching a state s_j from a state s_i in l time steps is given
 173 by $P^l(i, j)$, i.e. the l -th power of the transition matrix P . If a state s_j can be
 174 reached from a state s_i in a finite number of time steps and vice versa, i.e.
 175 $\exists l \in \mathbb{N} P^l(i, j) \geq 0 \wedge P^l(j, i) \geq 0$, the states s_i and s_j communicate. All states
 176 that communicate with each other are said to be in the same communication
 177 class. If all states of a state space are in the same communication class, i.e.
 178 if it is possible to reach every state from any other state in a finite number
 179 of time steps, the corresponding transition matrix P is called irreducible.

180 *2.2.2. Cyclic time-variant Markov process*

181 A cyclic Markov process with period T is described by T transition ma-
 182 trices P_r , one for each time of the day $r = 0, \dots, T - 1$. The probability of the
 183 process reaching state s_j from state s_i in l time steps at time $t = 0$ is given as
 184 $(P_0 \cdot \dots \cdot P_{T-1})^m \cdot P_0 \cdot \dots \cdot P_{r_l}(i, j)$ with $l = mT + r_l$. For an arbitrary time-step
 185 t , the formula must be multiplied from the left with the term $P_{r_t} \cdot \dots \cdot P_{T-1}$.
 186 Thus, the Markov process is irreducible, if the matrix $\mathbf{P} = P_0 \cdot \dots \cdot P_{T-1}$ is
 187 irreducible, i.e. if $\exists l \in \mathbb{N} \mathbf{P}^l(i, j) \geq 0 \forall i, j$.

188 *2.3. The stationary distribution*

If a Markov chain is irreducible and aperiodic then the long-term statistics
 of a Markov chain are described by the stationary probability distribution:
 $\pi = \lim_{t \rightarrow \infty} \alpha_0 P^t$. The distribution is independent of the initial distribution
 α_0 and satisfies the balance equation $\pi = \pi P$. By the Perron-Frobenius
 theorem it can be computed as the normalized eigenvector corresponding to
 the eigenvalue 1 of the transition matrix [17].

In the case of the cyclic time-inhomogeneous Markov process there is also
 a stationary distribution π_r , for all $r < T$. It can be interpreted as the limiting
 distribution of the Markov process considering only the datapoints sampled
 at time of the day r . If the matrix \mathbf{P} is irreducible, i.e. if $\exists \pi^*$, such that
 $\pi^* = \lim_{t \rightarrow \infty} \alpha_0 \cdot \mathbf{P}^t$ and the process is aperiodic, the stationary distribution
 π_r exists and is given by $\pi^* \cdot P_0 \cdot \dots \cdot P_{r-1}$, since it satisfies the balance
 equation 1:

$$\begin{aligned}
 \pi_r &= \pi^* \cdot P_0 \cdot \dots \cdot P_{r-1} \\
 \pi_r &= \pi^* \cdot \mathbf{P} \cdot P_0 \cdot \dots \cdot P_{r-1} \\
 \pi_r &= \pi^* \cdot P_0 \cdot \dots \cdot P_{r-1} \cdot P_r \cdot P_{r+1} \cdot \dots \cdot P_{T-1} \cdot P_0 \cdot \dots \cdot P_{r-1} \\
 \pi_r &= \pi_r \cdot (P_r \cdot P_{r+1} \cdot \dots \cdot P_{T-1} \cdot P_0 \cdot P_1 \cdot \dots \cdot P_{r-1}).
 \end{aligned} \tag{1}$$

189 *2.4. Persistence*

190 The persistence of a given state s_i is related with the number of steps
 191 the system consecutively remains in this state. In the time-homogeneous
 192 case, it follows a geometric distribution with expected value $(1 - p_{i,i})^{-1}$ and
 193 is denoted by τ . Anastasiou and Tsekos [1] showed that it is possible to
 194 determine the expected time that a Markov chain stays consecutively inside
 195 a given subset of states using a simple closed-form expression. For example, in
 196 wind power applications, a typical subset of interest could contain all states

197 corresponding to power production above a given threshold. To compute
 198 this estimate, the states are renumbered, s.th. they can be partitioned into
 199 two disjoint subsets: $\mathcal{A} = \{s_\nu, \dots, s_n\}$ containing the states of interest; and
 200 $\overline{\mathcal{A}} = \{s_0, \dots, s_{\nu-1}\}$, its complement. Then, the transition matrix is rearranged
 201 into the following block structure:

$$P = \begin{pmatrix} A & B \\ C & D \end{pmatrix} = \left[\begin{array}{ccc|ccc} p_{0,0} & \cdots & p_{0,\nu-1} & p_{0,\nu} & \cdots & p_{0,n} \\ \vdots & & \vdots & \vdots & & \vdots \\ p_{\nu-1,0} & \cdots & p_{\nu-1,\nu-1} & p_{\nu-1,\nu} & \cdots & p_{\nu-1,n} \\ \hline p_{\nu,0} & \cdots & p_{\nu,\nu-1} & p_{\nu,\nu} & \cdots & p_{\nu,n} \\ \vdots & & \vdots & \vdots & & \vdots \\ p_{n,0} & \cdots & p_{n,\nu-1} & p_{n,\nu} & \cdots & p_{n,n} \end{array} \right],$$

202 where the first and last block of rows and columns correspond to the
 203 states in subset $\overline{\mathcal{A}}$ and \mathcal{A} , respectively. The expected value of persistence,
 204 i.e. the expected number of time steps the Markov process consecutively
 205 remains in the subset \mathcal{A} once it is entered, is given by:

$$E\{\tau\} = \frac{\pi_{\mathcal{A}} \mathbf{1}_{\mathcal{A}}}{\pi_{\mathcal{A}} C \mathbf{1}_{\mathcal{B}}},$$

206 where $\pi_{\mathcal{A}}$ is the stationary probability distribution of the states in subset
 207 \mathcal{A} and $\mathbf{1}_{\mathcal{A}}$ is the unit column vector of size $(n - \nu + 1) \times 1$ [1].
 208 For the time-inhomogeneous case, persistence τ_t is defined as the number of
 209 time steps the Markov process is expected to remain in a state (set of states),
 210 once it is entered at time t . For a cyclic Markov process, the persistence τ_t
 211 is equal for all t that are congruent modulo T . Thus, it is only necessary
 212 to compute the persistence for τ_r , $r = 0, \dots, T - 1$. This can be achieved by
 213 adapting the derivation of equation 2.4, provided by Anastasiou and Tsekos
 214 [1], to time-variant cyclic Markov processes.
 215 After renaming, s.th. the subset of interest is $\mathcal{A} = \{s_\nu, \dots, s_n\}$, the states of
 216 each transition matrix P_r are rearranged as in equation 2.4.

$$P_r = \begin{pmatrix} A_r & B_r \\ C_r & D_r \end{pmatrix} = \left[\begin{array}{ccc|ccc} p_{0,0}(r) & \cdots & p_{0,\nu-1}(r) & p_{0,\nu}(r) & \cdots & p_{0,n}(r) \\ \vdots & & \vdots & \vdots & & \vdots \\ p_{\nu-1,0}(r) & \cdots & p_{\nu-1,\nu-1}(r) & p_{\nu-1,\nu}(r) & \cdots & p_{\nu-1,n}(r) \\ \hline p_{\nu,0}(r) & \cdots & p_{\nu,\nu-1}(r) & p_{\nu,\nu}(r) & \cdots & p_{\nu,n}(r) \\ \vdots & & \vdots & \vdots & & \vdots \\ p_{n,0}(r) & \cdots & p_{n,\nu-1}(r) & p_{n,\nu}(r) & \cdots & p_{n,n}(r) \end{array} \right],$$

217 The probability of τ_r to be equal to l is given as:

$$\begin{aligned} Pr(\tau_r = l) &= Pr(X_r \in \mathcal{A}, \dots, X_{r+l} \in \mathcal{A}, X_{r+l+1} \notin \mathcal{A} \mid X_r \in \mathcal{A}, X_{r-1} \notin \mathcal{A}) \\ &= \sum_{i \in \mathcal{A}} Pr(X_r = i \mid X_r \in \mathcal{A}, X_{r-1} \notin \mathcal{A}) \cdot Pr(X_s \in \mathcal{A}, r < s \leq l, X_{r+l+1} \notin \mathcal{A} \mid X_r = i) \\ &= \sum_{i \in \mathcal{A}} \sum_{k \notin \mathcal{A}} \sum_{j \in \mathcal{A}} \tilde{\pi}_r(i) \cdot \mathcal{P}_{i,j}(r, l-1, \mathcal{A}) \cdot p_{j,k}(r+l) \end{aligned} \quad (2)$$

218 with

$$\begin{aligned} \mathcal{P}_{i,j}(r, l, \mathcal{A}) &= Pr(X_{r+l} = j, X_k \in \mathcal{A}, 0 < k < l \mid X_r = i) \\ &= D_r \cdots D_{r+l-1} \cdot C_{r+l} \cdot \mathbf{1}_{\bar{\mathcal{A}}} \end{aligned}$$

219 and

$$\begin{aligned} \tilde{\pi}_r(i) &= Pr(X_r = i \mid X_r \in \mathcal{A}, X_{r-1} \notin \mathcal{A}) \\ &= \frac{\sum_{j \notin \mathcal{A}} Pr(X_r = i \mid X_{r-1} = j) \cdot Pr(X_{r-1} = j)}{\sum_{i \in \mathcal{A}} \sum_{j \notin \mathcal{A}} Pr(X_r = i \mid X_{r-1} = j) \cdot Pr(X_{r-1} = j)} \\ &= \frac{\sum_{j \notin \mathcal{A}} \pi_{r-1}(j) p_{j,i}(r-1)}{\sum_{k \in \mathcal{A}} \sum_{j \notin \mathcal{A}} \pi_{r-1}(j) p_{j,k}(r-1)}, \quad i \in \mathcal{A}, \end{aligned} \quad (3)$$

220 where $\pi_r(j)$ is the long term probability of occurrence (stationary proba-
221 bility) of state j at time of the day r ; also note that $\pi_t(j) = \pi_r(j)$ for $t = mr$,
222 $\forall m \in \mathbb{N}$. Equation 3 can be rewritten in the matrix form to include all states
223 in the subset \mathcal{A} :

$$\tilde{\pi}_r(\mathcal{A}) = \frac{\pi_{r-1}(\overline{\mathcal{A}}) \cdot B_{r-1}}{\pi_{r-1}(\overline{\mathcal{A}}) \cdot B_{r-1} \cdot \mathbf{1}_{\mathcal{A}}},$$

224 where $\mathbf{1}_{\mathcal{A}}$ is a unit vector of dimension $(n - \nu + 1) \times 1$ and $\pi_{r-1}(\overline{\mathcal{A}})$ is a
 225 vector of dimensions $1 \times \nu$, whose elements are the stationary probabilities
 226 of the states in the set $\overline{\mathcal{A}}$ at time of the day $r - 1$.

227 Thus, equation 2 can be rewritten as:

$$\begin{aligned} Pr(\tau_r = l) &= \tilde{\pi}_r(\mathcal{A}) \cdot D_r \cdot \dots \cdot D_{r+l-1} \cdot C_{r+l} \cdot \mathbf{1}_{\overline{\mathcal{A}}} \\ &= \frac{\pi_{r-1}(\overline{\mathcal{A}}) \cdot B_{r-1}}{\pi_{r-1}(\overline{\mathcal{A}}) \cdot B_{r-1} \cdot \mathbf{1}_{\mathcal{A}}} \cdot D_r \cdot \dots \cdot D_{r+l-1} \cdot C_{r+l} \cdot \mathbf{1}_{\overline{\mathcal{A}}}. \end{aligned}$$

228 The expected value of persistence at time r can then be derived as:

$$E(\tau_r) = \sum_{l=1}^{\infty} l \cdot \frac{\pi_{r-1}(\overline{\mathcal{A}}) \cdot B_{r-1}}{\pi_{r-1}(\overline{\mathcal{A}}) \cdot B_{r-1} \cdot \mathbf{1}_{\mathcal{A}}} \cdot D_r \cdot \dots \cdot D_{r+l-1} \cdot C_{r+l} \cdot \mathbf{1}_{\overline{\mathcal{A}}}$$

229 Making use of the cyclicity of the Markov process, this can be expressed
 230 as:

$$E(\tau_r) = \sum_{l=1}^{\infty} l \cdot \frac{\pi_{r-1}(\overline{\mathcal{A}}) \cdot B_{r-1}}{\pi_{r-1}(\overline{\mathcal{A}}) \cdot B_{r-1} \cdot \mathbf{1}_{\mathcal{A}}} \cdot \mathcal{D}^m \cdot D_r \cdot \dots \cdot D_{r+r_l-1} \cdot C_{r+r_l} \cdot \mathbf{1}_{\overline{\mathcal{A}}}$$

231 where $\mathcal{D} = D_r \cdot \dots \cdot D_T \cdot D_{T+1} \cdot \dots \cdot D_{r-1}$ and $l = mT + r_l$.

232

233 It can be seen that the sum converges after splitting it into T partial
 234 sums, one for each time of the day r . For each partial sum, the only term not
 235 constant is the matrix power \mathcal{D}^m , which converges because all \mathcal{D} eigenvalues
 236 are smaller than 1. The infinite sum for the expected value of persistence at
 237 time r can be approximated to an arbitrary degree of accuracy ϵ by defining

$$f_l = l \cdot \frac{\pi_{r-1}(\overline{\mathcal{A}}) \cdot B_{r-1}}{\pi_{r-1}(\overline{\mathcal{A}}) \cdot B_{r-1} \cdot \mathbf{1}_{\mathcal{A}}} \cdot \mathcal{D}^m \cdot D_r \cdot \dots \cdot D_{r+r_l-1} \cdot C_{r+r_l} \cdot \mathbf{1}_{\overline{\mathcal{A}}}.$$

238 and successively adding f_l , $l = 0, 1, \dots, L$ until the difference between two
 239 consecutive sums is smaller than ϵ , i.e. until $|f_L| < \epsilon$.

240 **3. Parameter estimation**

241 *3.1. Time-homogeneous Markov chain*

242 The common approach to estimate the Markov chain transition matrix
 243 P is through the optimization of a constrained maximum likelihood func-
 244 tion, which describes the realization probability of a given dataset [2]. For
 245 a sequence of M states $\{X_0 = s_{i_0}, \dots, X_M = s_{i_M}\}$ with $s_{i_0}, \dots, s_{i_M} \in S$
 246 and $i_0, \dots, i_M \in \{0, \dots, n\}$, its probability can be computed as $Pr\{X_0 =$
 247 $s_{i_0}\}p_{i_0,i_1}p_{i_1,i_2} \cdots p_{i_{M-1},i_M}$. Since the term $Pr\{X_0 = s_{i_0}\}$ is constant, given a
 248 set of observed state transitions \mathcal{S} , it is possible to estimate P by maximizing
 249 the likelihood

$$OF_1 = \prod_{(i,j) \in \mathcal{S}} p_{i,j}, \quad (4)$$

250 where a transition is described by an ordered pair (i, j) indicating the ori-
 251 gin and the destination of the transition. In practice, instead of maximizing
 252 OF_1 with respect to the $p_{i,j}$ variables it is preferable to minimize the nega-
 253 tive log-likelihood function, i.e. $-\log(OF_1)$, since it transforms the original
 254 mathematical programming problem into an equivalent one that is convex
 255 and, thus, has a unique solution [4]. The overall optimization problem is
 256 formulated as follows:

$$\begin{aligned} \min & & - \sum_{(i,j) \in \mathcal{S}} \log(p_{i,j}) \\ \text{subject to} & & p_{i,j} \geq 0 \quad \forall i, j = 0, \dots, n \\ & & \sum_j p_{i,j} = 1 \quad \forall i = 0, \dots, n \end{aligned}$$

257 The constraints ensure non-negativity of the transition probabilities and that
 258 they sum up to 1 for each row of the transition matrix.

259 *3.2. Cyclic time-variant Markov process*

260 The goal of this time-variant Markov process is to get a model that accu-
 261 rately reproduces the long-term behavior while considering the daily patterns
 262 observed in the data. Thus, the proposed objective function combines two
 263 maximum likelihood estimators: the first term maximizes the likelihood of

264 the cycle-average probability; and, the second term maximizes the likeli-
 265 hood of the time-dependent probability. The final optimization problem is
 266 transformed into a convex one using the negative logarithm of the objective
 267 function. This section provides a detailed description of the objective func-
 268 tion, the parametrization of the time-variant probability functions, and the
 269 constraints that must be added to the optimization problem to ensure its
 270 Markov properties.

271 3.2.1. Objective function

272 The transition probabilities are considered to be time-variant and cyclic
 273 with a period of T , i.e. for each time of the day r ($= 0, \dots, T - 1$) there is a
 274 different transition matrix P_r . In this paper, the time-dependent transition
 275 probabilities $p_{i,j}(r)$ are modeled by Bernstein polynomials. This has several
 276 advantages: a) a polynomial representation of the transition probabilities
 277 leads to a convex objective function and constraints, i.e. the optimization
 278 problem has a unique solution; b) a polynomial representation allows to de-
 279 crease the number of variables in the optimization problem: for each transi-
 280 tion, instead of T variables only $k + 1$ are needed for a k order polynomial; c)
 281 Bernstein polynomials are non-negative, which simplifies probability model-
 282 ing, when compared to other polynomial bases; and d) they have the convex
 283 hull property, which, combined with de Casteljaeu algorithm, allows to easily
 284 write probability boundary conditions.

285 Bernstein polynomials are linear combinations of Bernstein basis polynomi-
 286 als $b_{\mu,k}(z)$, $z \in [0, 1]$. The $k + 1$ Bernstein basis polynomials of order k are
 287 defined as:

$$b_{\mu,k}(z) = \binom{k}{\mu} z^{\mu}(1 - z)^{k-\mu}$$

288 with $\mu = 0, \dots, k$ and $\binom{k}{\mu}$ the binomial coefficient. Thus, the transition
 289 probabilities $p_{i,j}(z)$ are described by

$$p_{i,j}(z) = \sum_{\mu=0}^k \beta_{\mu}^{i,j} b_{\mu,k}(z),$$

290 with $\beta_{\mu}^{i,j} \in \mathbb{R}$ and $z = \frac{r}{T}$, since the polynomial variable has to be scaled,
 291 s.th. it is between 0 and 1.

292

293 Hence, to maximize the likelihood of the time-dependent transition prob-
 294 abilities given the data, the objective function must consider the time of the
 295 day z when the transition happens. Therefore, the objective function intro-
 296 duced in (4) becomes $\sum_{(i,j)_z \in \mathcal{S}_z} \log(p_{i,j}(z))$, where \mathcal{S}_z is the set of observed
 297 transitions together with the time z when they happens. This objective func-
 298 tion allows to compute the intra-cycle transition probability functions, and
 299 thus to represent the daily patterns present in the data.

300 A second term is added to this function, namely $\sum_{(i,j) \in \mathcal{S}} \log(p_{i,j}^{avg})$, where
 301 \mathcal{S} is the set of transitions observed in the data as defined in section 3.1 and
 302 $p_{i,j}^{avg}$ is the cycle-average (daily) probability of transition from state s_i to s_j .
 303 It can be computed as follows:

$$\begin{aligned} p_{i,j}^{avg} &= \frac{1}{1-0} \int_0^1 p_{ij}(z) dz = \int_0^1 \sum_{\mu=0}^k \beta_k^{i,j} b_{\mu,k}(z) dz \\ &= \sum_{\mu=0}^k \beta_k^{i,j} \int_0^1 b_{\mu,k}(z) dz = \frac{1}{k+1} \sum_{\mu=0}^k \beta_k^{i,j} \end{aligned}$$

304 This second term is the maximum likelihood estimator for the daily av-
 305 erage probability and its addition to the objective function increases the
 306 consistency of the long-term behavior of the Markov process with the data.
 307 Therefore, the overall objective function OF_2 is given by:

$$\begin{aligned} OF_2 &= - \sum_{(i,j) \in \mathcal{S}} \log(p_{i,j}^{avg}) - \sum_{(i,j)_z \in \mathcal{S}_z} \log(p_{i,j}(z)) \\ &= - \sum_{(i,j) \in \mathcal{S}} \log\left(\frac{1}{k+1} \sum_{\mu=0}^k \beta_k^{i,j}\right) - \sum_{(i,j)_z \in \mathcal{S}_z} \log\left(\sum_{\mu=0}^k \beta_\mu^{i,j} b_{\mu,k}(z)\right) \end{aligned}$$

308 and minimization is performed with respect to the coefficients $\beta_\mu^{i,j}$ (model
 309 parameters).

310 3.2.2. Constraints

311 The estimation of the model parameters requires the transition probabil-
 312 ity functions to comply with several constraints, to ensure:

- 313 • \mathcal{C}^0 - and \mathcal{C}^1 -continuity at $z = 0$,

- 314 • row-stochasticity of the transition matrices at every time of the day z
- 315 and
- 316 • that the transition probability functions are non-negative and bounded
- 317 by 1.

318 Thus, to complete the specification of the optimization problem this section
 319 explains all the necessary constraints required for the model parameters to
 320 describe a cyclic Markov process.

321 *Periodicity*

322 The transition probability functions are modeled using Bernstein polyno-
 323 mials, which are smooth, i.e. \mathcal{C}^∞ -continuous functions. In general, the values
 324 at both ends of their domain (0 and 1) need not be equal. Thus, to avoid
 325 sudden changes in the value and slope of each probability function between
 326 the cycles, two constraints are added to ensure \mathcal{C}^0 and \mathcal{C}^1 -continuity. An-
 327 other reason is the arbitrariness of the cycle starting position, which affects
 328 the position of the discontinuity if these conditions are not used.

329 The first constraint is $p_{i,j}(0) = p_{i,j}(1)$. Since $b_{\mu,k}(0) = \delta_{\mu,0}$ and $b_{\mu,k}(1) =$
 330 $\delta_{\mu,k}$ the constraint can be reformulated as $\beta_0^{i,j} = \beta_k^{i,j}$, where δ is the Kronecker
 331 delta. The second constraint is added to ensure \mathcal{C}^1 -continuity, i.e. $\frac{dp_{i,j}}{dz}(0) =$
 332 $\frac{dp_{i,j}}{dz}(1)$. The first derivative of a Bernstein basis polynomial can be written
 333 as a combination of two polynomials of lower degree:

$$\frac{db_{\mu,k}}{dz}(z) = k(b_{\mu-1,k-1}(z) - b_{\mu,k-1}(z))$$

334 Thus, the first derivative of a transition probability $p_{i,j}(z)$ is given by:

$$\frac{dp_{i,j}}{dz}(z) = k\left(\sum_{\mu=1}^k (\beta_\mu^{i,j} - \beta_{\mu-1}^{i,j})b_{\mu-1,k-1}(z) - \beta_k^{i,j}b_{k,k-1}(z)\right)$$

335 Hence, using $b_{\mu,k}(0) = \delta_{\mu,0}$ and $b_{\mu,k}(1) = \delta_{\mu,k}$ as well as the first constraint
 336 $\beta_0^{i,j} = \beta_k^{i,j} \forall i, j = 0, \dots, n$, the constraint $\frac{dp_{i,j}}{dz}(0) = \frac{dp_{i,j}}{dz}(1)$ reduces to the
 337 following linear constraint:

$$\beta_k^{i,j} = \beta_0^{i,j} = 0.5(\beta_1^{i,j} + \beta_{k-1}^{i,j})$$

338 *Row stochasticity of transition matrices*

339 To ensure row stochasticity of the time-variant transition matrices, it is
 340 necessary to ensure that $\sum_j p_{i,j}(z) = 1$ for all i and z . Since the Bernstein
 341 basis polynomials of order k form a partition of unity, i.e.

$$\sum_{\mu=0}^k b_{\mu,k}(z) = 1$$

342 the constraint can be re-written as a linear combination of the polynomial
 343 coefficients:

$$\begin{aligned} \sum_j p_{i,j}(z) = 1 &\Leftrightarrow \sum_j \sum_{\mu=0}^k \beta_{\mu}^{i,j} b_{\mu,k}(z) = 1 \\ &\Leftrightarrow \sum_j \beta_{\mu}^{i,j} = 1 \end{aligned}$$

344 *Non-negative transition probabilities are bounded by 1*

345 The most straightforward way to implement this constraint is to add two
 346 inequalities for each time of the day and each transition probability $p_{i,j}$, i.e.

$$\begin{aligned} p_{i,j}(z) &\geq 0 \quad \forall i, j, z \\ p_{i,j}(z) &\leq 1 \quad \forall i, j, z \end{aligned} \tag{5}$$

347 However, this constraint significantly increases the problem size, since it
 348 requires $2 \cdot T \cdot n^2$ inequalities. An alternative constraint can be formulated by
 349 using the convex hull property of the Bernstein polynomials. This constraint
 350 makes the overall optimization problem size smaller, but is more restrictive.

351 Every Bernstein polynomial $\sum_{\mu=0}^k \beta_{\mu} b_{\mu,k}(z)$ always lies in the convex hull
 352 defined by its control points $(\frac{k}{\mu}, \beta_{\mu})$, $\mu = 0, \dots, k$. Thus the constraint

$$0 \leq p_{i,j}(z) \leq 1 \quad \forall i, j = 0, \dots, n$$

353 can be reformulated in terms of the polynomial coefficients as

$$0 \leq \beta_{\mu}^{i,j} \leq 1 \quad \forall \mu = 0, \dots, k \tag{6}$$

354 Since constraint 6 is a sufficient but not necessary condition for con-
 355 straint 5, the reformulation leads to a more restrictive overall minimization

356 problem, i.e. the optimum objective function value is always higher or equal
357 when compared with the problem with original constraint 5. The convex
358 hull bound of Bernstein polynomials can be tightened by subdivision, i.e.
359 by subdividing the domain in two regions and finding new control points
360 $\beta_0^{i,j}(1), \dots, \beta_k^{i,j}(1)$ and $\beta_{k+1}^{i,j}(1), \dots, \beta_{2k}^{i,j}(1)$ such that the function output re-
361 mains unchanged. With each subdivision, the control points form a tighter
362 bound around the polynomial and thus the polynomial coefficients can as-
363 sume values in a wider range. The new control points represent the polyno-
364 mial restricted to the two sub-intervals $[0, z^*]$ and $[z^*, 1]$, where $z^* \in [0, 1]$
365 is the cutting point of the division. For simplicity, z^* is fixed to 0.5 in all
366 transition probabilities. The new control points can be determined by linear
367 combinations of the original control points $\beta_0^{i,j}, \dots, \beta_k^{i,j}$. This can be performed
368 efficiently using de Casteljau algorithm, which in matrix form is given as:

$$\begin{pmatrix} \beta_0^{i,j}(1) \\ \vdots \\ \beta_k^{i,j}(1) \end{pmatrix} = \begin{pmatrix} b_{0,0}(z^*) & 0 & \cdots & 0 \\ b_{0,1}(z^*) & b_{1,1}(z^*) & \cdots & 0 \\ \vdots & \vdots & \ddots & \vdots \\ b_{0,k}(z^*) & b_{1,k}(z^*) & \cdots & b_{k,k}(z^*) \end{pmatrix} \begin{pmatrix} \beta_0^{i,j} \\ \vdots \\ \beta_k^{i,j} \end{pmatrix} = C_l \begin{pmatrix} \beta_0^{i,j} \\ \vdots \\ \beta_k^{i,j} \end{pmatrix} = C_l \cdot \beta^{i,j} \quad (7)$$

369 and

$$\begin{pmatrix} \beta_{k+1}^{i,j}(1) \\ \vdots \\ \beta_{2k}^{i,j}(1) \end{pmatrix} = \begin{pmatrix} b_{0,k}(z^*) & b_{1,k}(z^*) & \cdots & b_{k,k}(z^*) \\ 0 & b_{0,k-1}(z^*) & \cdots & b_{k-1,k-1}(z^*) \\ \vdots & \vdots & \ddots & \vdots \\ 0 & \cdots & 0 & b_{0,0}(z^*) \end{pmatrix} \begin{pmatrix} \beta_0^{i,j} \\ \vdots \\ \beta_k^{i,j} \end{pmatrix} = C_r \begin{pmatrix} \beta_0^{i,j} \\ \vdots \\ \beta_k^{i,j} \end{pmatrix} = C_r \cdot \beta^{i,j} \quad (8)$$

370 The subdivision can be applied recursively to further improve the convex
371 bound around the polynomial. The corresponding coefficients are computed
372 by applying equations 7 and 8 to the left and right coefficient vectors. Defin-
373 ing $C = (C_l, C_r)^T$ and I_z as the identity matrix of dimension $z \times z$, the
374 coefficients $\beta^{i,j}(w) = (\beta_0^{i,j}(w), \dots, \beta_{2^w k}^{i,j}(w))$ after w subdivisions can be ob-
375 tained by:

$$\beta^{i,j}(w) = (C \otimes I_{2^{w-1}}) \cdot (C \otimes I_{2^{w-2}}) \cdot \dots \cdot (C \otimes I_2) \cdot (C \otimes I_1) \cdot \beta^{i,j}$$

376 where \otimes denotes the Kronecker product. The number of inequalities
377 needed for the implementation of this constraint is $(k+1) \cdot 2^{\omega+1} \cdot n^2$. Thus,

378 its use only makes sense if it decreases the problem size, i.e. for a number of
 379 subdivisions ω such that $(k + 1) \cdot 2^{\omega+1} \leq T$.

380 3.2.3. Problem formulation

381 The overall optimization problem to be solved for the estimation of the
 382 transition probability coefficients $\beta_\mu^{i,j}$ can be written as:

$$\min_{\beta_\mu^{i,j}} \quad - \sum_{(i,j) \in \mathcal{S}} \log\left(\frac{1}{k+1} \sum_{\mu=0}^k \beta_\mu^{i,j}\right) - \sum_{(i,j)_z \in \mathcal{S}_z} \log\left(\sum_{\mu=0}^k \beta_\mu^{i,j} b_{\mu,k}(z)\right) \quad (9)$$

$$\text{subject to} \quad \beta_0^{i,j} = \beta_k^{i,j} \quad \forall i, j = 1, \dots, n \quad (10)$$

$$\beta_0^{i,j} = 0.5(\beta_1^{i,j} + \beta_{k-1}^{i,j}) \quad \forall i, j = 0, \dots, n \quad (11)$$

$$\sum_j \beta_\mu^{i,j} = 1 \quad \forall i = 0, \dots, n; \forall \mu = 0, \dots, k \quad (12)$$

$$\beta^{i,j}(w) \leq 1 \quad \forall i, j = 0, \dots, n \quad (13)$$

$$0 \leq \beta^{i,j}(w) \quad \forall i, j = 0, \dots, n \quad (14)$$

383 where w is the number of subdivisions and k is the order of the Bern-
 384 stein polynomials, which have to be specified. The objective function (9) is
 385 a combination of two negative log-likelihood functions to ensure the Markov
 386 process captures both the daily patterns and the long-term behavior of the
 387 original data. The optimization is performed with respect to several con-
 388 straints: constraints (10) and (11) ensure \mathcal{C}^0 - and \mathcal{C}^1 -continuity at $z = 0$.
 389 The row-stochasticity of the transition matrix is ensured by constraint (12).
 390 The last two constraints (13) and (14) bound the transition probabilities
 391 between 0 and 1.

392 It is expected that the objective function decreases with the polynomial
 393 order and the number of subdivisions. The parameters of the Markov chain
 394 model $\beta_\mu^{i,j}$ are estimated by solving the optimization problem using a rigor-
 395 ous numerical solver. The model was formulated making use of the casadi
 396 computation framework [3] and the optimization was performed by ipopt, a
 397 nonlinear interior-point solver [27], which ensures convergence to the global
 398 optimum in the case of convex optimization problems.

399 **4. Application of the cyclic Markov process to wind turbine mod-**
400 **eling**

401 *4.1. The data*

402 The data for this study was obtained from a wind power turbine in a
403 wind park located in a mountainous region in Portugal. The time series
404 consists of a three-year period (2009-2011) of historical data gotten from the
405 turbine data logger. The sampling time of 10 minutes leads to 144 samples
406 each day. The data-set comprises three variables, wind power, speed and
407 direction (nacelle orientation). The wind speed information was collected
408 from the anemometer placed in the wind turbine hub. Due to confidentiality,
409 wind power and speed data values are reported as a fraction of the rated
410 power and the cut-out speed, respectively.

411 *4.2. Markov chain state definition*

412 Discrete Markov chain models require the definition of the states when
413 applied to describe continuous variables. This work proposes to characterize
414 the wind turbine states using three different variables: wind power, speed and
415 direction. As such, each state is defined by all the points inside a polyhedron
416 in three-dimensional space.

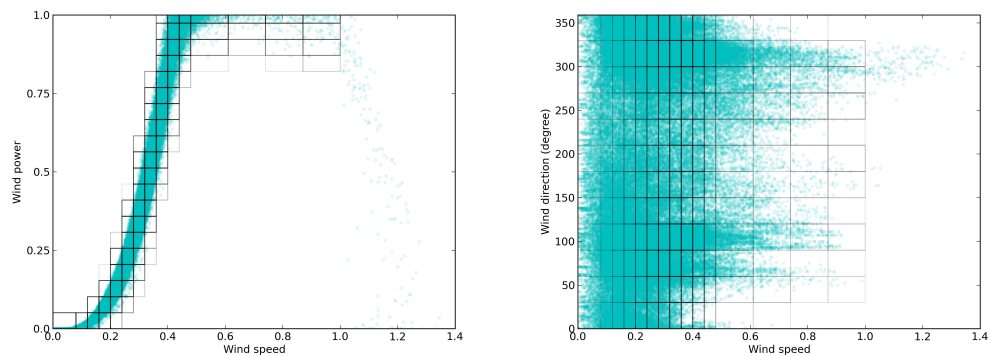


Figure 1: Representation of all data points projected into the: a) wind direction and speed plane (left); and, b) wind power and speed plane (right). Each rectangle is the projection of a state polyhedron into the two planes. Overall, they define the final state partition for the three-dimensional variable space.

417 Fig. 1 presents all data observations and the state partitions projected
418 into: a) the wind direction and speed plane; and, b) the wind power and

419 speed plane. As expected, the observations projected into the wind power
 420 and speed plane define the characteristic power curve of the wind turbine.
 421 It shows the three operational regions of a wind turbine: a) below the cut-in
 422 speed no power is produced; b) between cut-in and rated wind speed the
 423 power increases proportionally to the cube of wind speed; c) at wind speeds
 424 between the rated and the cut-out wind speed, the turbine control system
 425 limits the power output to a constant value. In the wind direction and speed
 426 plane, data is widely scattered and shows the dominant wind patterns at the
 427 site. Three accumulation regions can be identified: one for low wind speeds,
 428 centered on 0.25, which is the mode of the wind speed, and two defining the
 429 dominant wind directions around 100° and 300° .

430 The data space is discretized unevenly to get a good resolution of the high-
 431 slope region of the power curve. In a previous work [13], this partition was
 432 used in a time-homogeneous Markov chain and proved to lead to an accurate
 433 representation of the original data. The wind direction and power are divided
 434 by an equally spaced grid leading to 12 ($\{d_1, \dots, d_{12}\}$) and 20 ($\{p_1, \dots, p_{20}\}$)
 435 classes, respectively. The wind speed is divided as follows: values below the
 436 cut-in speed define one class sp_1 ; between the cut-in and rated wind speed
 437 the discretization is narrowed by selecting 10 classes ($\{sp_2, \dots, sp_{11}\}$); and be-
 438 tween the rated and cut-out wind speed discretization is widened and 4 classes
 439 ($\{sp_{12}, \dots, sp_{15}\}$) are defined. Data points with wind speed above the cut-out
 440 wind speed are discarded. The complete state set is constructed by listing
 441 all possible combinations of the classes of each variable. Due to physical
 442 constraints between the variables, most of the states are empty (fig. 1(left))
 443 and can be discarded. This reduces the number of states from 3840 to 778,
 444 for this turbine.

445 *4.3. Additional transitions to promote a single communication class*

446 The solution of the optimization problem described in section 3 comprises
 447 a set of transition matrices P_r , $r \in \{0, \dots, 143\}$. However, the constraints in
 448 the optimization problem definition do not force the matrix $\mathbf{P} = P_0 \cdot \dots \cdot P_{143}$
 449 to be irreducible and thus the Markov process to have a single communication
 450 class. So, during data synthesis, the Markov process can get “trapped”
 451 within a communication class. To induce the Markov process to have a
 452 single communication class, additional transition counts are introduced into
 453 the data. The goal is to add a small set of transitions to promote state
 454 connectivity without distorting the original data. Thus, the set is composed
 455 of transitions that connect neighboring states in the state space, since those

456 are the ones most likely to occur.

457 For a state $s_i = (p_l, sp_p, d_q)$, its neighborhood V is defined as

$$V(s_i) := \{(p_{ll}, sp_{pp}, d_{qq}) : ll \in \{l-1, l, l+1\}, pp \in \{p-1, p, p+1\}, qq \in \{q-1, q, q+1\}\} \setminus s_i. \quad (15)$$

458

459 It should be noted that, unlike power and speed, direction is a circular
 460 variable, e.g. states d_0 and d_{11} are considered neighbors. If a neighbor state
 461 $s_j \in V(s_i)$ is present in the dataset, a transition (i, j) is added to the set
 462 of extra transitions \mathcal{S}_E . For this dataset, originally consisting of 150601
 463 transitions, 13610 transitions are added.

464 The extra transitions must be considered to happen at an unknown time of
 465 the day z . Thus, they can only be accounted for in the objective function
 466 term without time information, i.e. only in the time-variant part of the
 467 objective function. This directly affects the values for $p_{i,j}^{avg}$ and, indirectly,
 468 the model parameters. Since the aim is to cause a minimal impact on the
 469 transition probabilities, the additional term is weighed by a factor $\omega < 1$
 470 to directly control its influence. In this work it is fixed to 0.05. Thus, the
 471 following term is added to the objective function:

$$-\omega \cdot \sum_{(i,j) \in \mathcal{S}_E} \log(p_{i,j}^{avg}) = -\omega \cdot \sum_{(i,j) \in \mathcal{S}_E} \log\left(\frac{1}{k+1} \sum_{\mu=0}^k \beta_k^{i,j}\right) \quad (16)$$

472 Although the use of the extra transition set does not ensure the time-
 473 variant Markov process to have a single communication class, results show a
 474 decrease of the number of communication classes from 13 to 1 in this dataset.

475 5. Simulation of wind power, speed and direction time series

476 To simulate wind power, speed and direction time series the method de-
 477 scribed by Sahin and Sen [22] is adapted to the cyclic time-variant Markov
 478 model as follows. First, the cumulative probability transition matrices P_r^{cum}
 479 with $P_r^{cum}(i, j) = \sum_{k=0}^j p_{i,k}(r)$ are computed. Then an initial state s_i , i.e.
 480 $X_0 = s_i$, is randomly selected. A new datapoint X_{t+1} is generated by uni-
 481 formly selecting a random number ϵ between zero and one. The correspond-
 482 ing state s_{new} ($X_{t+1} = s_{new}$) is chosen such that the probability of reaching
 483 it from the current state s_i is bigger than ϵ , i.e. such that $P_{r_t}^{cum}(i, new) \geq \epsilon$.
 484 Based on this discrete state sequence, a real value for the wind power/speed/direction
 485 variables is generated by sampling each state partition uniformly.

486 **6. Results and discussion**

487 *6.1. Daily patterns in the data*

488 The wind power, speed and direction time-series clearly show a daily
489 time-dependent behavior.

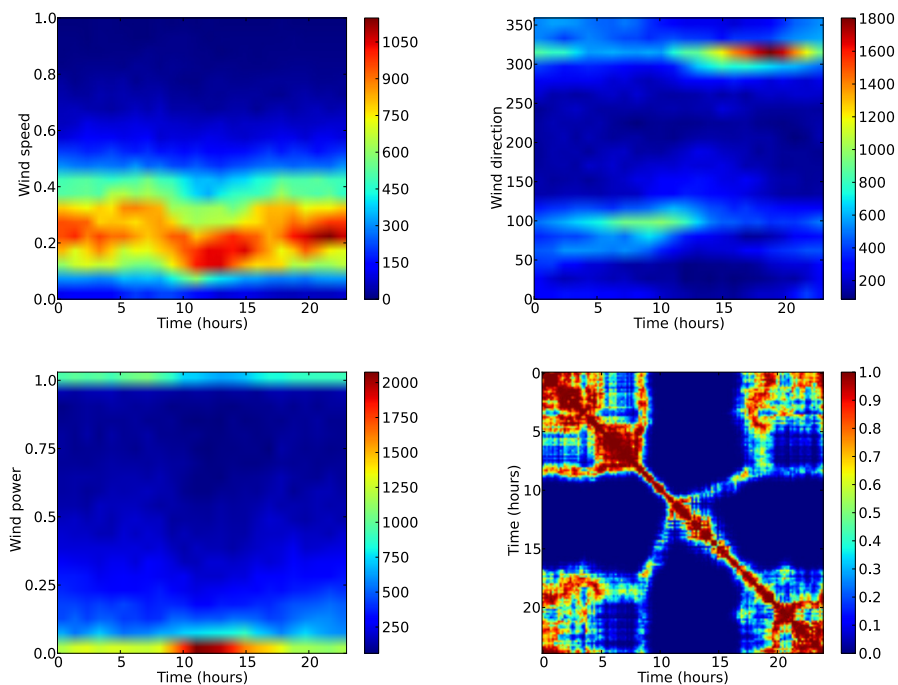


Figure 2: Two-dimensional histograms of the original time series data: speed-time (top left), direction-time (top right) and power-time (bottom left). The subfigure on the bottom right shows the p-value of the Kolmogorov-Smirnov test used to compare the wind speed distribution on the different times of the day.

490 Figure 2 shows that, on average, the turbine does not produce power
491 between 10 am and 3 pm. In this time interval, low wind speeds (0.1 - 0.25)
492 are the most likely events. There are two dominant wind directions: around
493 100° and 300° . Moreover, they occur at specific times of the day; between 5
494 and 10am, the wind typically blows from the 100° direction, the rest of the
495 day from 300° .

496 To assess whether these two dominant directions might be due to sum-
497 mer/winter seasonality, the dataset was divided in two subsets, one covering
498 the period from April to September and the other from October to March.
499 The histogram analysis shows that both, summer and winter subset, have the
500 same two dominant directions (figures not shown). Thus, it was concluded
501 that the time-dependent pattern is not induced by this seasonality.

502 Figure 2 bottom-right plot shows the p-values of the Kolmogorov-Smirnov
503 test applied to the wind speed distributions at different times of the day. The
504 Kolmogorov-Smirnov test is a nonparametric test for the equality of con-
505 tinuous one-dimensional probability distributions. Thus, the high p-values
506 around the diagonal illustrates that wind speed distributions for consecutive
507 times of the day are similar. The same holds for wind speeds in the morning
508 and evening, i.e. before 9am and after 4:30pm. The wind speed distribution
509 between 10am and 3pm is clearly different.

510 *6.2. Choice of polynomial order and number of subdivisions*

511 The model introduced in section 3.2 has two parameters that need to
512 be defined: k , the order of the Bernstein polynomials used to model the
513 transition probabilities; and w , the number of subdivisions used to tighten
514 the convex hull that bounds the polynomials. To choose proper values for
515 these parameters, different models were computed by varying $k = 4..10$
516 and $w = 0..3$. For each model, synthetic data was generated following the
517 procedure described in section 5 and compared with the real dataset.

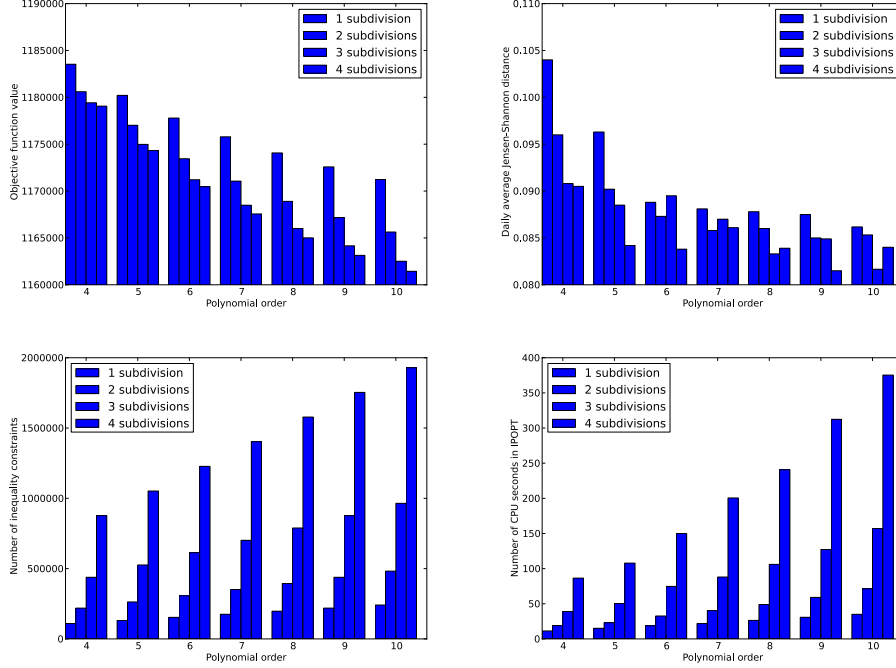


Figure 3: Bar plots comparing the objective function value (top left), the daily average Jensen-Shannon distance between original and synthesized data (top right), the number of inequalities in the problem formulation (bottom left) and the CPU time spent in IPOPT solving the optimization problem (bottom right) of the tested models.

518 Figure 3 shows bar plots comparing the different models using four criteria:
519 the objective function value, the daily average Jensen-Shannon distance
520 between original and synthesized wind direction data, the number of inequalities
521 in the problem formulation and the CPU time spent in IPOPT solving
522 the optimization problem. The Jensen-Shannon distance is the square root
523 of the Jensen-Shannon divergence d_{js} , which, for two discrete probability
524 distributions q_1 and q_2 is defined as:

$$d_{js} = \frac{1}{2} \sum_i \frac{q_1(i)}{q_2(i)} \cdot q_1(i) + \frac{1}{2} \sum_i \frac{q_2(i)}{q_1(i)} \cdot q_1(i).$$

525 Comparing the models using the objective function value (figure 3 top
526 left) shows a decrease of the objective function as the model order and the

527 number of subdivisions increase. It can be seen that the impact of the number
 528 of subdivisions is higher for models with higher polynomial order. Moreover,
 529 the first subdivision has the highest impact since it leads to the highest
 530 decrease of the objective function value. The daily average of the Jensen-
 531 Shannon distance (figure 3 top right) decreases with the polynomial order
 532 until sixth order. The same behavior can be observed for the number of
 533 subdivisions: until the sixth order, the Jensen-Shannon distance decreases
 534 with the number of subdivisions. The number of inequality constraints in
 535 the optimization problem as well as the number of CPU seconds spent in the
 536 solver show the expected behavior (figure 3 bottom). They increase linearly
 537 with the polynomial order and exponentially with the number of subdivisions.
 538 Based on these observations, a basis order of 6 with 2 subdivisions was chosen
 539 as the best trade-off between an accurate representation of the average daily
 540 patterns and computational costs.

541 6.3. Capturing long-term statistics

542 This section compares the main statistical properties derived from the
 543 original data with the ones derived from the data generated by the time-
 544 variant Markov model.

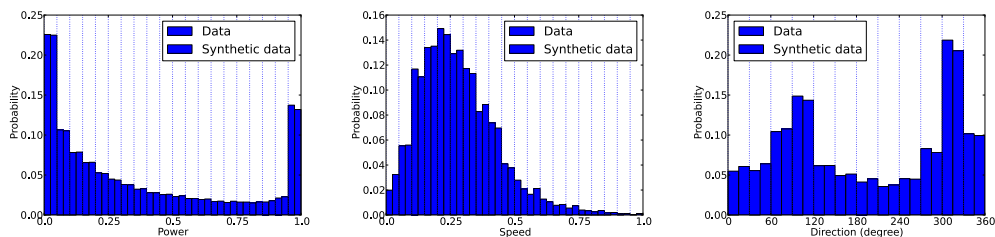


Figure 4: Comparison of the probability distribution of wind power (left),
 wind speed (middle) and wind direction (right) of the original with the syn-
 thesized data.

545 Figure 4 compares the wind power (left), speed (middle) and direction
 546 (right) distribution of the original with the synthetic data generated using
 547 the Markov model. In general, the distributions are in close agreement. The
 548 wind power distribution is bimodal, with the modes located at the minimum
 549 and maximum power. It shows that the intermediary power levels are rather
 550 rare, for instance, the states corresponding to a power production between
 551 0.4 and 0.9 have a low probability. The wind speed distribution follows the

552 expected behavior, a single mode distribution with a long tail for the high
 553 wind speeds (Weibull distribution). The wind direction distribution is bi-
 554 modal with the two modes at 100 and 300 degrees, which are the prevailing
 555 wind directions at the turbine site (figure 2).

556

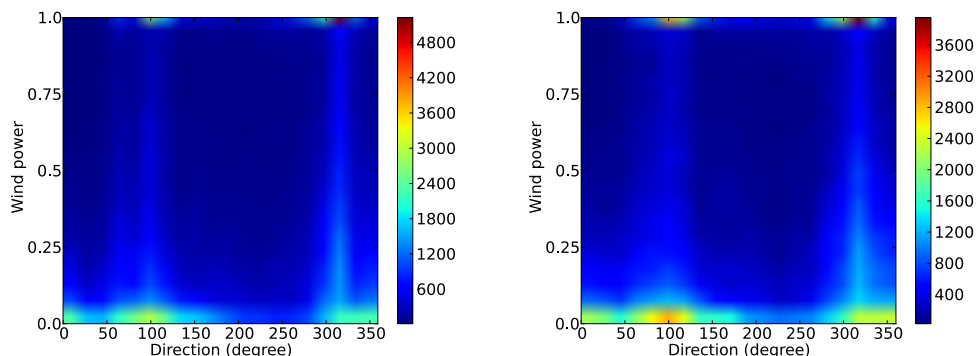


Figure 5: Two dimensional power-time histograms of the original (left) and synthetic (right) time-series data.

557 Figure 5 shows two plots: on the left, the empirical 2D distribution of
 558 the wind power and direction computed from the data and, on the right,
 559 the same distribution computed using the data generated by the Markov
 560 model. Its comparison shows that the model captures the joint statistics for
 561 the wind power and direction from the data. It is possible to see the two
 562 dominant directions associated with high wind power production, namely
 563 the sectors from 100 to 120 and from 290 to 320 degree. Figures 2 and 5
 564 clearly demonstrate the capability of this Markov model to capture the com-
 565 bined characteristics of the wind power, speed and direction. The long-term
 566 behavior of the model is close to what is observed in the dataset.

567 6.4. Capturing time-dependent behavior

568 As shown in section 6.1, the original data clearly exhibits a time-dependent
 569 behavior. To test, if the time-dependent Markov model can capture it, syn-
 570 thetic data was generated and the histograms compared to the ones of the
 571 original data. Moreover, to obtain a comparison with the “regular” way of
 572 data synthesis with Markov models, data was also generated from the time-
 573 invariant Markov chain.

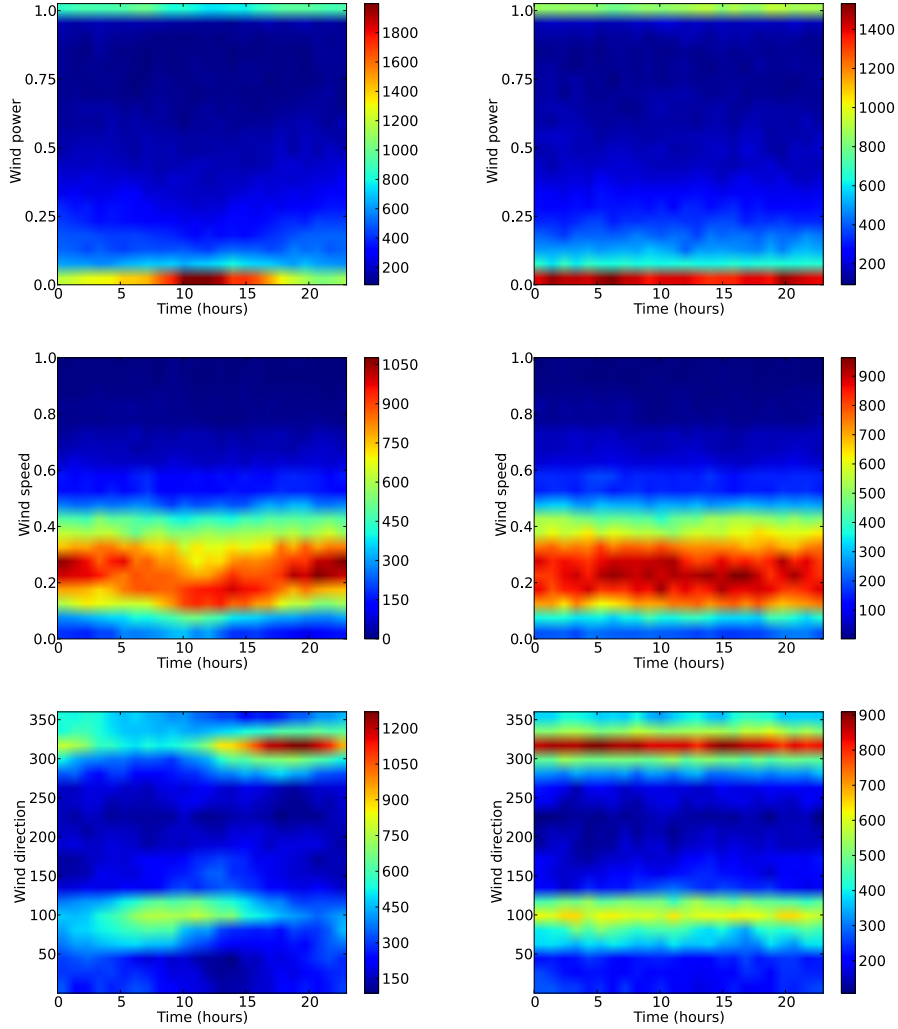


Figure 6: Two dimensional histograms of the synthetic time-series data, generated with the time-variant Markov model (left) and the time-invariant Markov chain (right): power-time (top), speed-time (middle) and direction-time (bottom).

574 The comparison of figures 2 and 6(first column) shows, that the time-
 575 variant Markov model is capable of reproducing the time-variant behavior
 576 of the data. Figure 6(second column) presents the results of using a time-
 577 invariant Markov chain model, i.e. by using constant transition probability

578 functions. As expected, each variable statistic distribution remains constant
579 during the daily cycle.

580 6.5. Time-dependent persistence of production

581 The time-dependent Markov model allows to compute the persistence of
582 power-production depending on the time of the day. Figure 6 shows the
583 time-dependent persistence of power production for different power levels
584 ($i \cdot 0.05 \cdot p_{max}$, for $i = 1, \dots, 19$). The persistence analysis is presented for two
585 power production levels: a) persistence of useful power production (PUPP)
586 defined as above $0.15 \cdot p_{max}$, i.e. the power level corresponding to the wind
587 speed mode at the turbine site; and, persistence for high power production
588 (PHPP), i.e. above $> 0.7 \cdot p_{max}$. It can be seen, that the higher the power
589 level, the lower the persistence. Moreover, for all power levels, persistence is
590 minimal between 5 and 10 am. PHPP is fairly constant throughout the day
591 (dark line), the maximal differences are between 10 and 30 minutes, whereas
592 PUPP reaches a maximum at around 5 pm (white line).

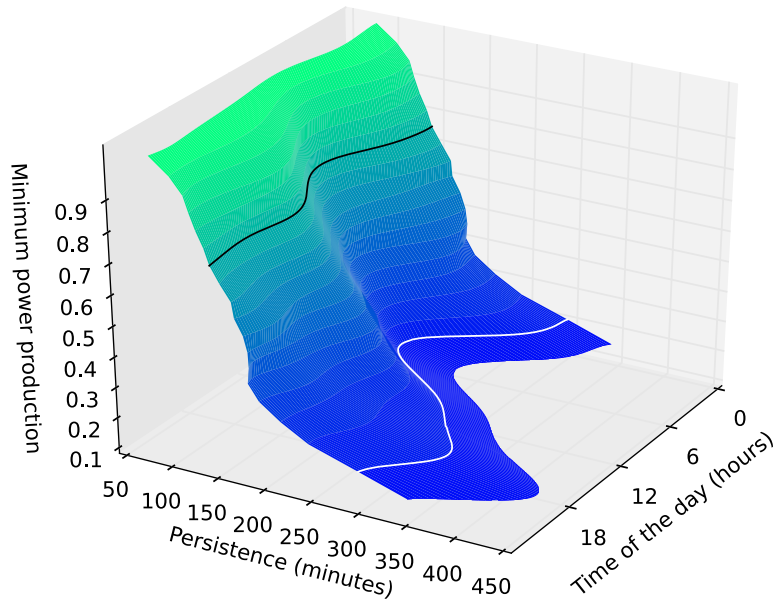


Figure 7: Time-dependent persistence of power production above $i \cdot 0.05 \cdot p_{max}$, for $i = 1, \dots, 19$. The lines highlight the time-dependent persistence, for two conditions: a) in white, for power production above $0.15 \cdot p_{max}$ (PUPP); and, b) in black, the power production above $0.7 \cdot p_{max}$ (PHPP).

593 Since the data shows two different dominant directions (figure 4), figure 8
 594 presents the persistence of power production conditioned to each dominant
 595 direction, i.e. for the direction sectors from 90° to 180° and 270° to 360° .

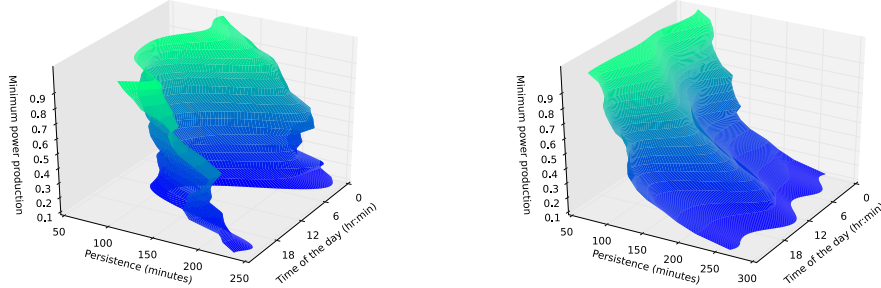


Figure 8: Time-dependent persistence of power production above $i \cdot 0.05 \cdot p_{max}$, for $i = 1, \dots, 19$ for direction sectors 90° - 180° (left) and 270° - 360° (right).

596 As expected, the persistence in both direction sectors is lower than the
 597 unconditioned persistence. For wind directions in the sector 90° - 180° , all
 598 levels of power production have a minimum persistence between 80 and 100
 599 minutes at around 1 pm. Maximum persistence is around midnight varying
 600 between 220 minutes (PUPP) and 140 minutes (PHPP). It can be seen that
 601 for power levels below 50% of maximum production the time of day depen-
 602 dency of persistence is very similar. For power levels above 50% persistence
 603 decreases as power production increases. However, the persistence variability
 604 with the power level is rather low, for example, maximum persistence at a
 605 level of 75% is almost 180 minutes whereas for a level above 0.05% is 200
 606 minutes.

607 For wind directions in the sector 270° - 360° , it shows that, for all power lev-
 608 els, the curves for both PUPP and PHPP are similar, i.e. their minima and
 609 maxima are located around the same time of the day. For instance, maximal
 610 persistence of production is reached at around midday. However, for this
 611 direction sector, the higher the power production level, the lower the persis-
 612 tence. For power production above 0.05% of maximum power the persistence
 613 is 250 minutes, persistence of production above 75% of maximum power is
 614 only 100 minutes.

615 Comparing with the other dominant direction, it can be seen, that they have
 616 very different persistence behavior. The maxima and minima are at different
 617 times of the day for every power level. The persistence increases as power
 618 production decreases, for all power levels in the case of the 270° - 360° sec-
 619 tor. For the 90° - 180° sector it decreases only until 50% of maximum power

620 production. Below that, it remains approximately constant.

621 **7. Conclusions**

622 This paper presents an inhomogeneous Markov process to model wind
623 power production. It is developed using states, which combine information
624 about the wind speed, direction and power variables, using real data recorded
625 by a wind turbine in Portugal. The joint partition of the three-dimensional
626 variable space allows to decrease the number of the model states and, si-
627 multaneously, encodes the wind power curve into the Markov chain model.
628 The transition probabilities are considered to be functions that depend on the
629 time of the day and modeled as Bernstein polynomials. The estimation of the
630 transition matrices is performed by solving a constrained convex optimiza-
631 tion problem. Its objective function combines two log-likelihood functions
632 with the purpose to accurately represent both the long-term behavior and
633 the daily fluctuations seen in the original data. To evaluate the statistical
634 properties of the estimated Markov model, synthetic time-series are gener-
635 ated and compared with the original data statistics. Results demonstrate
636 that the proposed Markov model can reproduce the diurnal patterns in the
637 data. Moreover it is demonstrated how the persistence of power production
638 throughout the time of the day can be estimated from the Markov process
639 transition matrices.

640 **Acknowledgments**

641 The authors thank the Fundação para a Ciência e a Tecnologia for fi-
642 nancial support (SFRH/BD/86934/2012, FCOMP-01-0124-FEDER-016080
643 (PTDC/SENENR/1141718/2009)) and GENERG, SA.

644 **References**

- 645 [1] Anastasiou, K., Tsekos, C., 1996. Persistence statistics of marine envi-
646 ronmental parameters from markov theory, part 1: analysis in discrete
647 time. *Applied Ocean Research* 18 (4), 187 – 199.
- 648 [2] Anderson, T. W., Goodman, L. A., 1957. Statistical inference about
649 markov chains. *The Annals of Mathematical Statistics* 28 (1), 89–110.
- 650 [3] Andersson, J., Houska, B., 2010. Towards a Computer Algebra System
651 with Automatic Differentiation for use with Object-Oriented modelling
652 languages. *Object-Oriented Modeling Languages*.
- 653 [4] Boyd, S. P., Vandenberghe, L., 2004. *Convex optimization*. Cambridge
654 Univ Pr.
- 655 [5] Cancino-Solórzano, Y., Gutiérrez-Trashorras, A. J., Xiberta-Bernat, J.,
656 2010. Analytical methods for wind persistence: Their application in
657 assessing the best site for a wind farm in the state of Veracruz, Mexico.
658 *Renewable Energy* 35 (12), 2844 – 2852.
- 659 [6] Carapellucci, R., Giordano, L., 2013. The effect of diurnal profile and
660 seasonal wind regime on sizing grid-connected and off-grid wind power
661 plants. *Applied Energy* 107 (0), 364 – 376.
- 662 [7] Chen, P., Berthelsen, K., Bak-Jensen, B., Chen, Z., 2009. Markov model
663 of wind power time series using Bayesian inference of transition matrix.
664 In: *Industrial Electronics, 2009. IECON '09. 35th Annual Conference of*
665 *IEEE*. pp. 627 –632.
- 666 [8] Corotis, R. B., Sigl, A. B., Klein, J., 1978. Probability models of wind
667 velocity magnitude and persistence. *Solar Energy* 20 (6), 483 – 493.
- 668 [9] Kemeny, J. G., Snell, J. L., 1976. *Finite Markov Chains*. New York :
669 Springer-Verlag.
- 670 [10] Koçak, K., 2002. A method for determination of wind speed persistence
671 and its application. *Energy* 27 (10), 967 – 973.
- 672 [11] Koçak, K., 2008. Practical ways of evaluating wind speed persistence.
673 *Energy* 33 (1), 65 – 70.

- 674 [12] Koçak, K., 2009. Examination of persistence properties of wind speed
675 records using detrended fluctuation analysis. *Energy* 34 (11), 1980 –
676 1985.
- 677 [13] Lopes, V. V., Scholz, T., Estanqueiro, A., Novais, A. Q., 2012. On
678 the use of Markov chain models for the analysis of wind power time-
679 series. In: *Environment and Electrical Engineering (EEEIC), 2012 11th*
680 *International Conference on*. pp. 770 –775.
- 681 [14] Masseran, N., Razali, A., Ibrahim, K., Zin, W. W., 2012. Evaluating the
682 wind speed persistence for several wind stations in peninsular Malaysia.
683 *Energy* 37 (1), 649 – 656.
- 684 [15] Nfaoui, H., Essiarab, H., Sayigh, A., 2004. A stochastic Markov chain
685 model for simulating wind speed time series at Tangiers, Morocco. *Re-*
686 *newable Energy* 29 (8), 1407 – 1418.
- 687 [16] Papaefthymiou, G., Klöckl, B., 2008. MCMC for wind power simulation.
688 *Energy Conversion, IEEE Transactions on* 23 (1), 234 –240.
- 689 [17] Pillai, S., Suel, T., Cha, S., 2005. The perron-frobenius theorem: some
690 of its applications. *Signal Processing Magazine, IEEE* 22 (2), 62–75.
- 691 [18] Platis, A., Limnios, N., Le Du, M., 1998. Dependability analysis of
692 systems modeled by non-homogeneous Markov chains. *Reliability Engi-*
693 *neering and System Safety* 61 (3), 235 – 249.
- 694 [19] Poje, D., 1992. Wind persistence in Croatia. *International Journal of*
695 *Climatology* 12 (6), 569–586.
- 696 [20] Pryor, S., Barthelmie, R., 2002. Statistical analysis of flow character-
697 istics in the coastal zone. *Journal of Wind Engineering and Industrial*
698 *Aerodynamics* 90 (3), 201 – 221.
- 699 [21] Raischel, F., Scholz, T., Lopes, V. V., Lind, P. G., 2012. Uncovering
700 wind turbine properties through two-dimensional stochastic modeling
701 of wind dynamics. Unpublished results, arXiv:1210.7161.
- 702 [22] Sahin, A. D., Sen, Z., 2001. First-order Markov chain approach to wind
703 speed modelling. *Journal of Wind Engineering and Industrial Aerody-*
704 *namics* 89 (34), 263 – 269.

- 705 [23] Shamshad, A., Bawadi, M., Hussin, W. W., Majid, T., Sanusi, S., 2005.
706 First and second order markov chain models for synthetic generation of
707 wind speed time series. *Energy* 30 (5), 693 – 708.
- 708 [24] Sigl, A. B., Corotis, R. B., Won, D. J., 1978. Run duration analysis
709 of surface wind speeds for wind energy application. *Journal of Applied*
710 *Meteorology* 18, 156–166.
- 711 [25] Suomalainen, K., Silva, C., ao, P. F., Connors, S., 2013. Wind power de-
712 sign in isolated energy systems: Impacts of daily wind patterns. *Applied*
713 *Energy* 101 (0), 533 – 540.
- 714 [26] Suomalainen, K., Silva, C., Ferro, P., Connors, S., 2012. Synthetic wind
715 speed scenarios including diurnal effects: Implications for wind power
716 dimensioning. *Energy* 37 (1), 41 – 50.
- 717 [27] Wächter, A., Biegler, L. T., 2006. On the implementation of an interior-
718 point filter line-search algorithm for large-scale nonlinear programming.
719 *Mathematical Programming* 106, 25–57.
- 720 [28] Wen, J., Zheng, Y., Donghan, F., 2009. A review on reliability assess-
721 ment for wind power. *Renewable and Sustainable Energy Reviews* 13 (9),
722 2485 – 2494.